Supporting Information

Experiment Section

Materials characterizations. X-ray diffraction (XRD) was used to characterize the crystallographic information and interlayer spacing of all catalysts on the X′Pert PRO MPD instrument with a scanning rate of 5° min-1 and a 2θ range of 3-95°. Scanning electron microscopy (SEM) images were used to characterize the morphology and nanostructures of all catalysts on the Hitachi S-4800 instrument. The morphology and elemental distribution of the catalyst were characterized by transmission electron microscopy (TEM) and the corresponding elemental energy dispersive X-rays (EDX) elemental mapping on a JEM-F200 instrument with an acceleration voltage of 20 kV. X-ray photoelectron spectroscopy (XPS) was used to study the valence state of the catalyst using AXIS SUPRA at 15 mA and 14 kV monochromatic A1 Ka sources.

Electrochemical measurements. All electrochemical tests were performed at the Gamry Reference 3000 electrochemical station, and a three-electrode system was set up in 1.0 M KOH for testing. The saturated calomel electrode (SCE) and graphite electrode were used as reference electrodes and counter electrodes, respectively. The working electrode was the synthetic catalyst for this load. The carbon paper was ultrasonically treated with ethanol and deionized water three times before use. In this work, all measured potentials are regulated by a reversible hydrogen electrode (RHE), calculated by the correlation formula E (RHE) = E (SCE) + 0.24 V+0.0592*pH. All electrochemical properties were tested by linear sweep voltammetry (LSV), and the LSV data curve was obtained at a scan rate of 5 mV s^{-1}. To test the charge transfer rate of the catalyst, electrochemical impedance spectroscopy (EIS) measurements were performed in the frequency window range of 0.1 ~ 100 kHz, and voltages of-1.219 V and 0.5 V were applied to the HER and OER tests, respectively. The cyclic voltammetry (CV) test was measured in the non-Faraday part. In this work, the scanning speed of the CV was set to 40 to 200 mV s^{-1}. The long-term stability test was performed by the chronoamperometry i-t method.

Supporting Figures and Tables

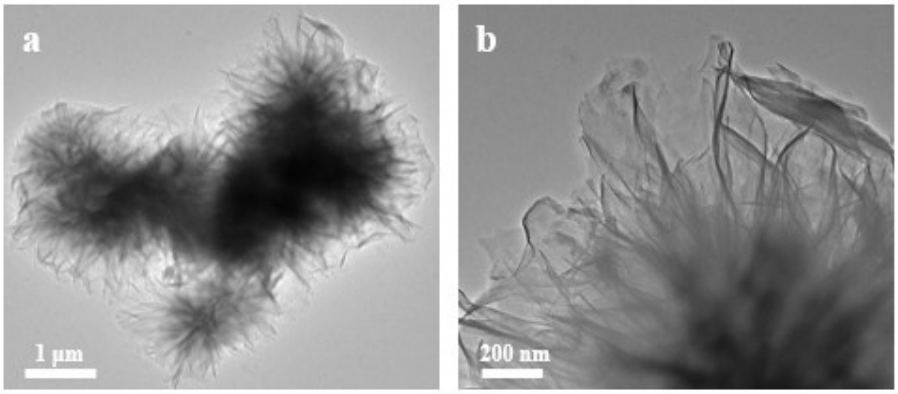

Fig. S1 TEM images of FeCo-LDH

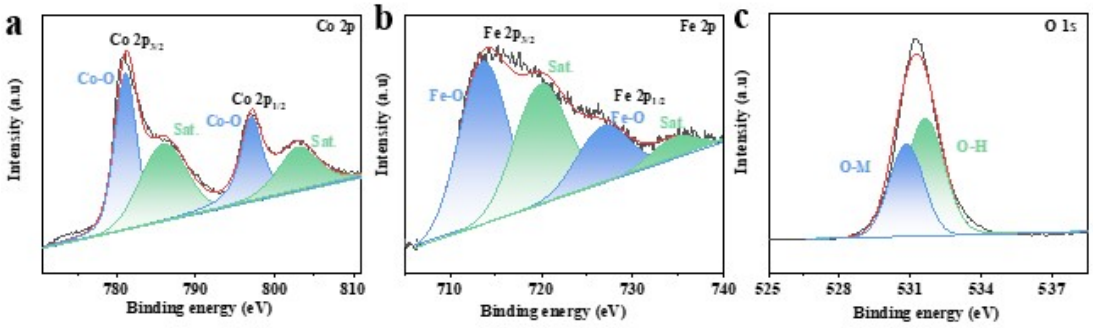

Fig. S2 (a) Co 2p, (b) Fe 2p, and (c) O 1s XPS spectra of FeCo-LDH.

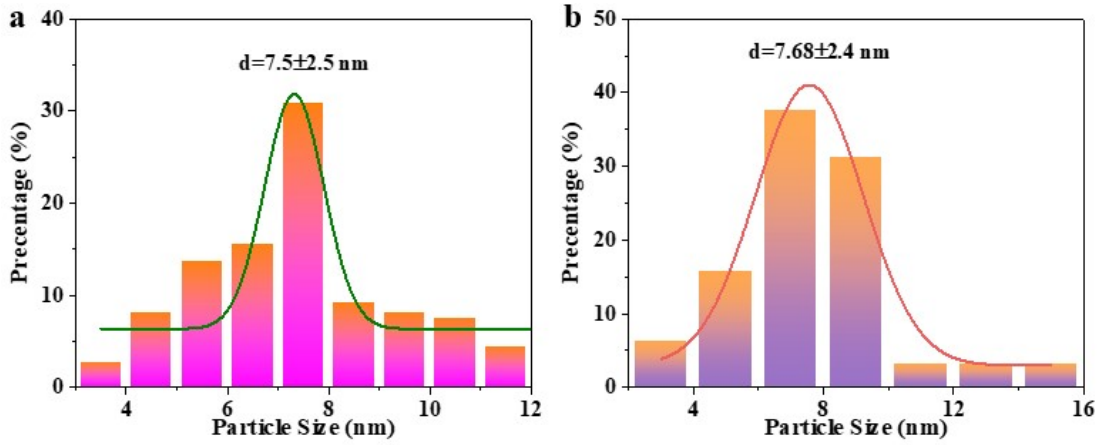

Fig.S3 (a) Size distribution diagram of Ru NPs on FeCo-LDH nanosheets. (b) Size distribution diagram of Ru NPs on FeCoP nanosheets.

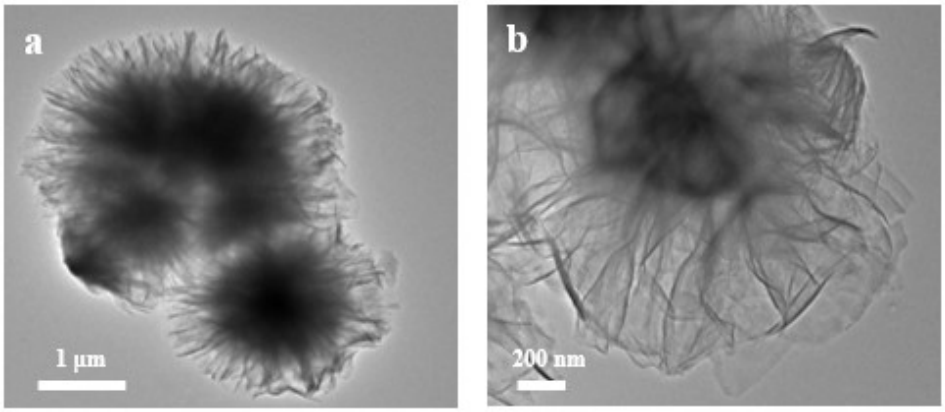

Fig. S4 TEM images of FeCoP.

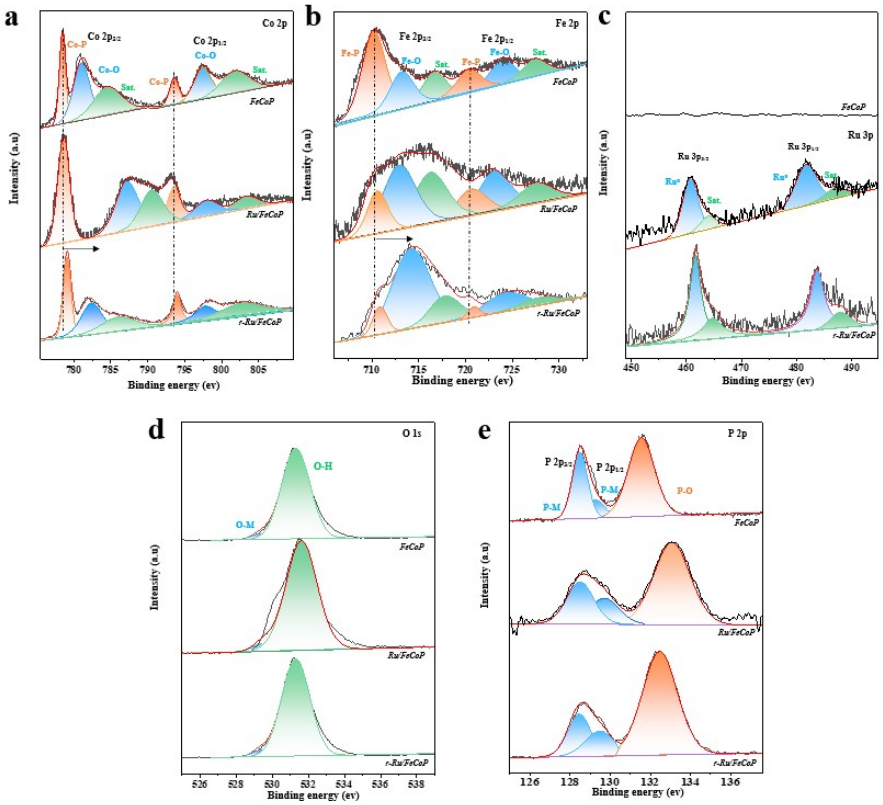

Fig. S5 (a) Co 2p, (b) Fe 2p, (c) Ru 3p, (d) O 1s, and (e) P 2p XPS spectra of r-Ru/FeCoP, Ru/FeCoP and FeCoP.

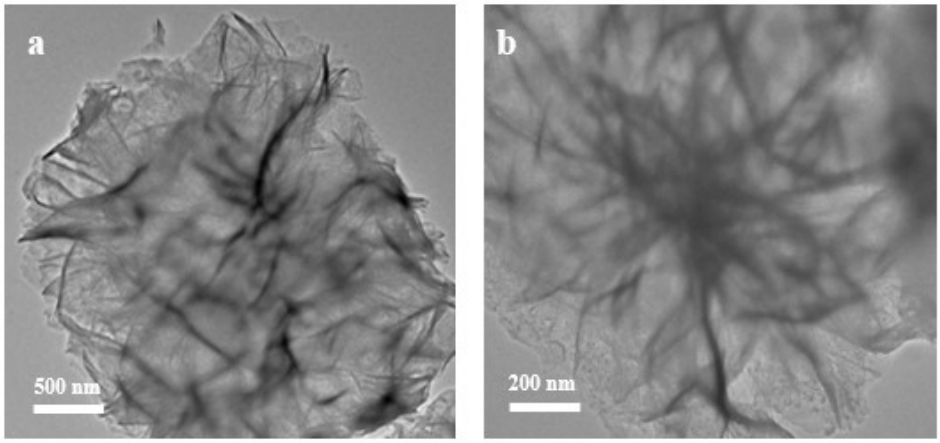

Fig. S6 TEM images of Ru/FeCoP.

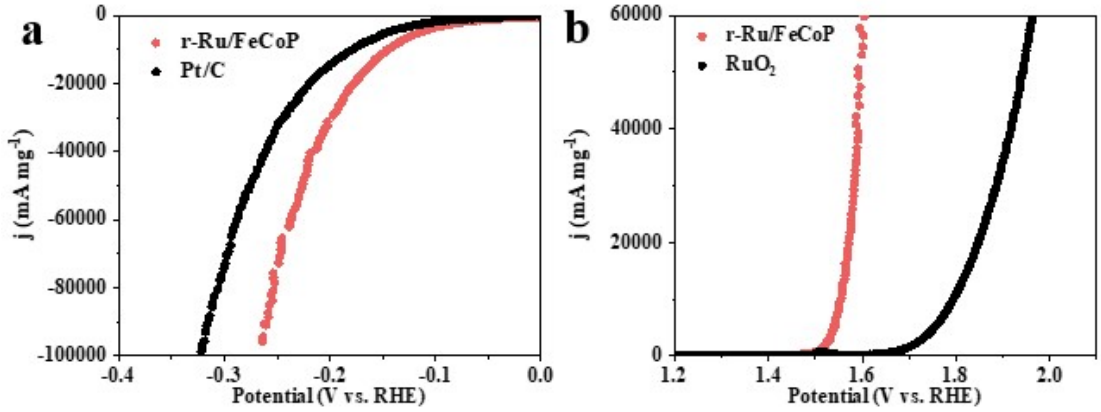

Fig.S7 (a) mass activity of r-Ru/FeCoP and Pt/C for HER in 1.0 M KOH. (b) mass activity of r-Ru/FeCoP and RuO2 for OER in 1.0 M KOH.

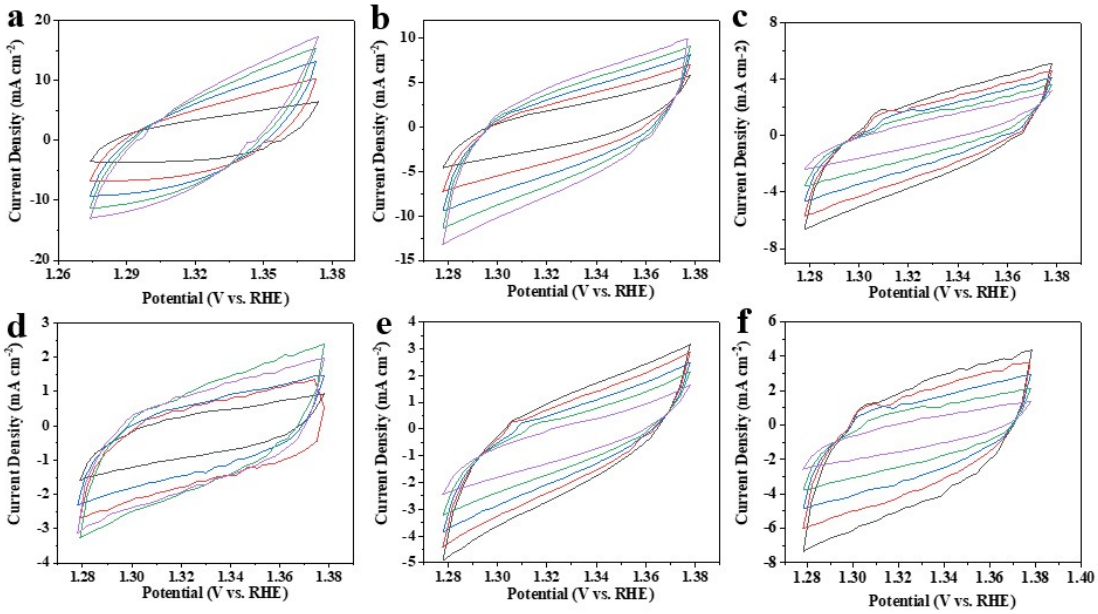

Fig. S8 Cyclic voltammograms of (a) r-Ru/FeCoP, (b) r-Ru/FeCo-LDH, (c) Ru/FeCoP, (d) FeCoP, (e) r-Ru/FeCoP-1h, (f) r- Ru/FeCoP-3h at 1.26-1.38 V vs RHE at 40-200 mV s^{-1} scan rate.

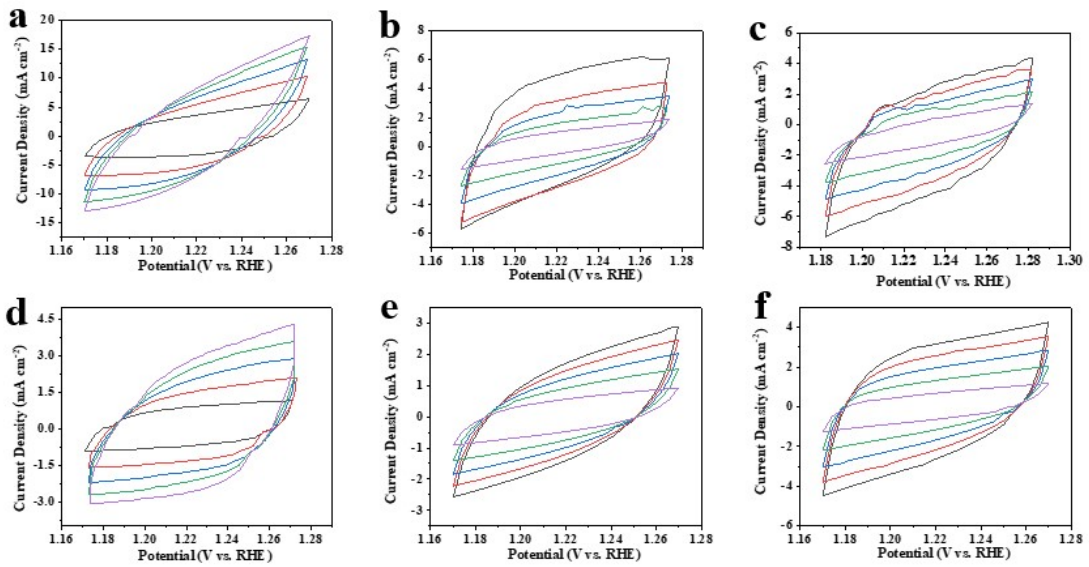

Fig. S9 Cyclic voltammograms of (a) r-Ru/FeCoP, (b) r-Ru/FeCo-LDH, (c) Ru/FeCoP, (d) FeCoP, (e) r-Ru/FeCoP-1h, (f) r- Ru/FeCoP-3h at 1.16-1.30 V vs RHE at 40-200 mV s^{-1} scan rate.

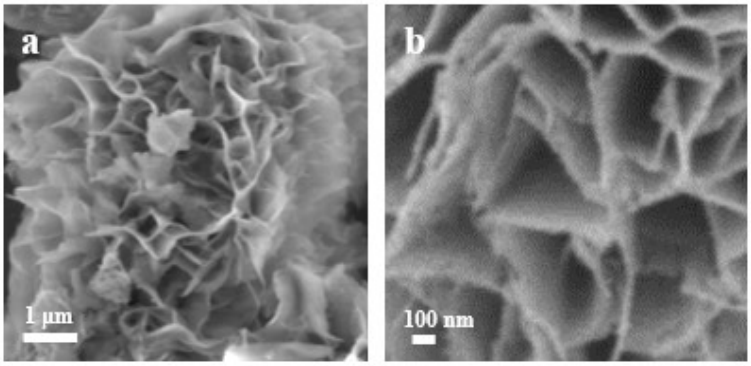

Fig. S10 SEM images of r-Ru/FeCoP after HER reaction.

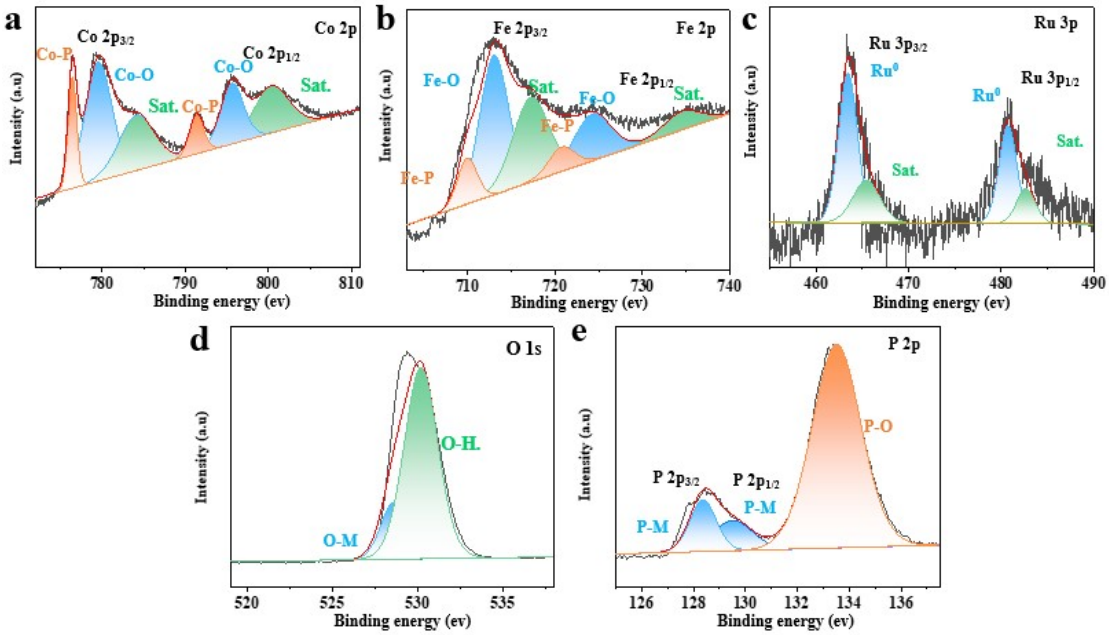

Fig. S11 (a) Co 2p, (b) Fe 2p, (c) Ru 3p, (d) O 1s, and (e) P 2p XPS spectra of r-Ru/FeCoP after HER reaction.

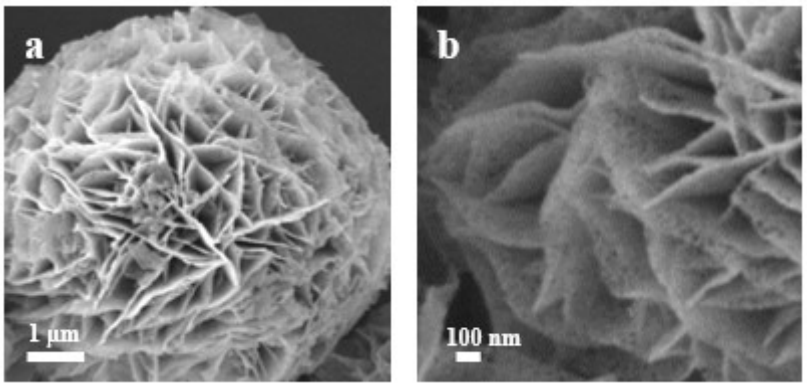

Fig. S12 SEM images of r-Ru/FeCoP after OER reaction.

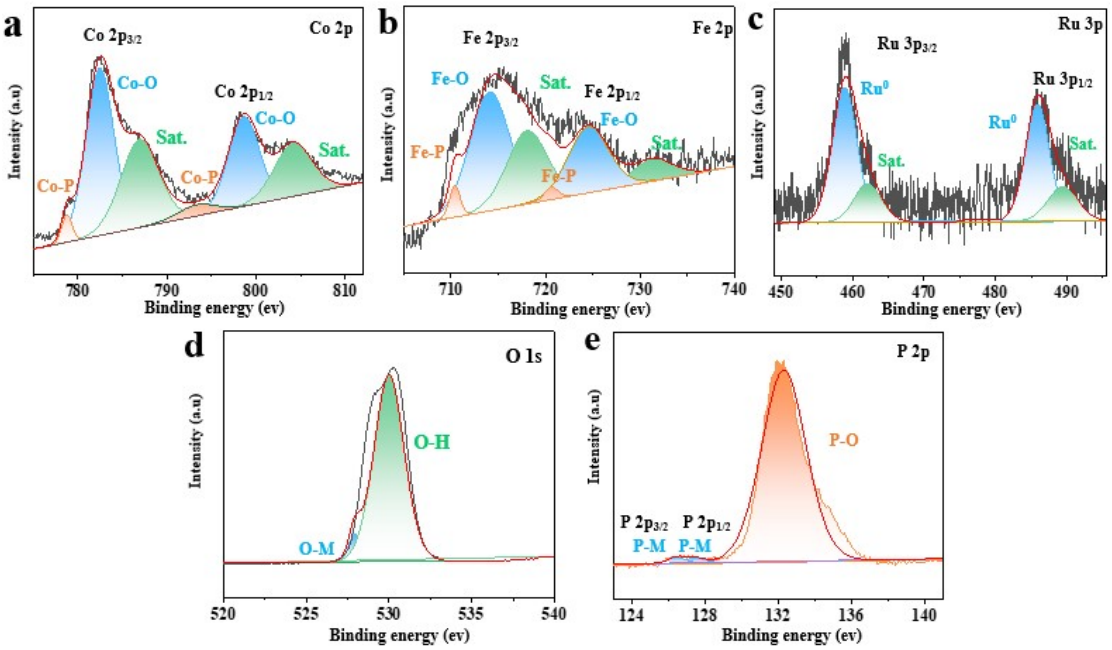

Fig. S13 (a) Co 2p, (b) Fe 2p, (c) Ru 3p, (d) O 1s, and (e) P 2p XPS spectra of r-Ru/FeCoP after OER reaction.

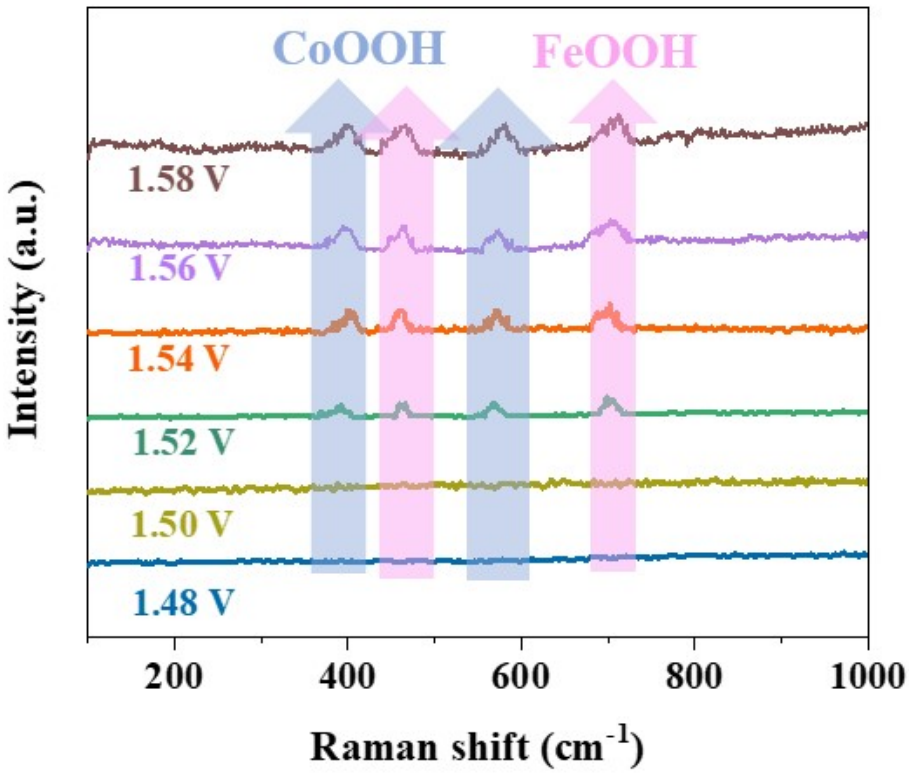

Fig. S14 In situ Raman spectra of r-Ru/FeCoP.

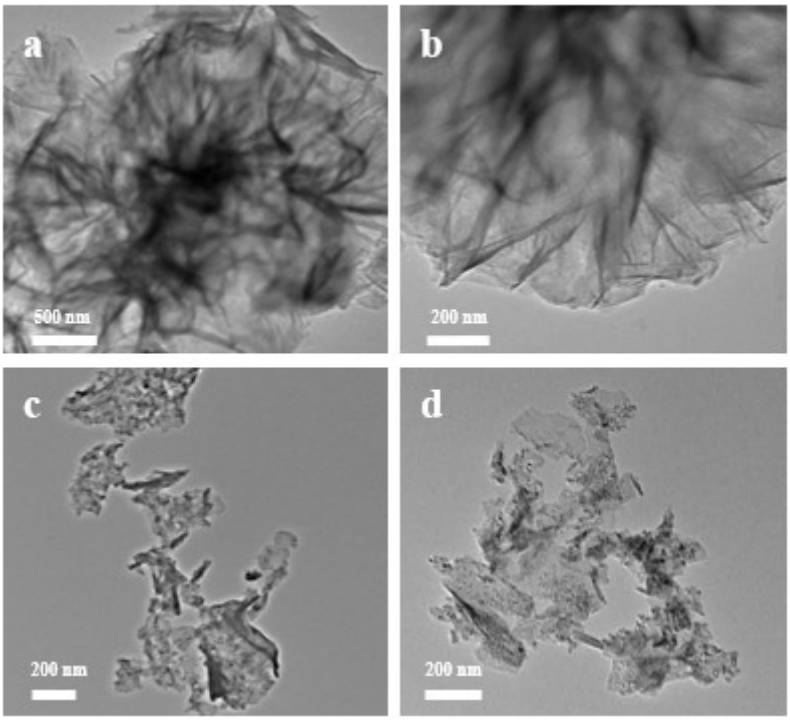

Fig. S15 (a, b) TEM images of r-Ru/FeCoP-1h. (c, d) TEM images of r-Ru/FeCoP-3h.

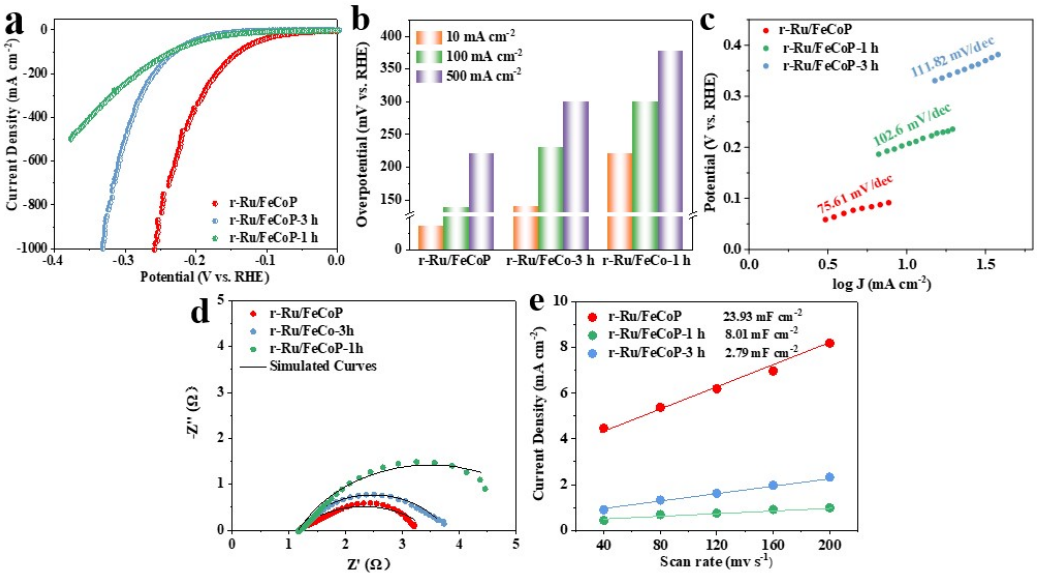

Fig. S16 HER is manifested in 1.0 M KOH. (a) The HER polarization curves of r-Ru/FeCoP, r-Ru/FeCoP-1h, r-Ru/FeCoP-3h in 1.0 M KOH. (b) η_{10}, η_{100}, η_{500} overpotential comparison. (c) Tafel plots of r-Ru/FeCoP, r-Ru/FeCoP-1h, r-Ru/FeCoP-3h. (d) Nyquist plots of r-Ru/FeCoP, r-Ru/FeCoP-1h, r-Ru/FeCoP-3h. (e) The curves of the scanning rate of r-Ru/FeCoP, r-Ru/FeCoP-1h, and r-Ru/FeCoP-3h with capacitance current are shown.

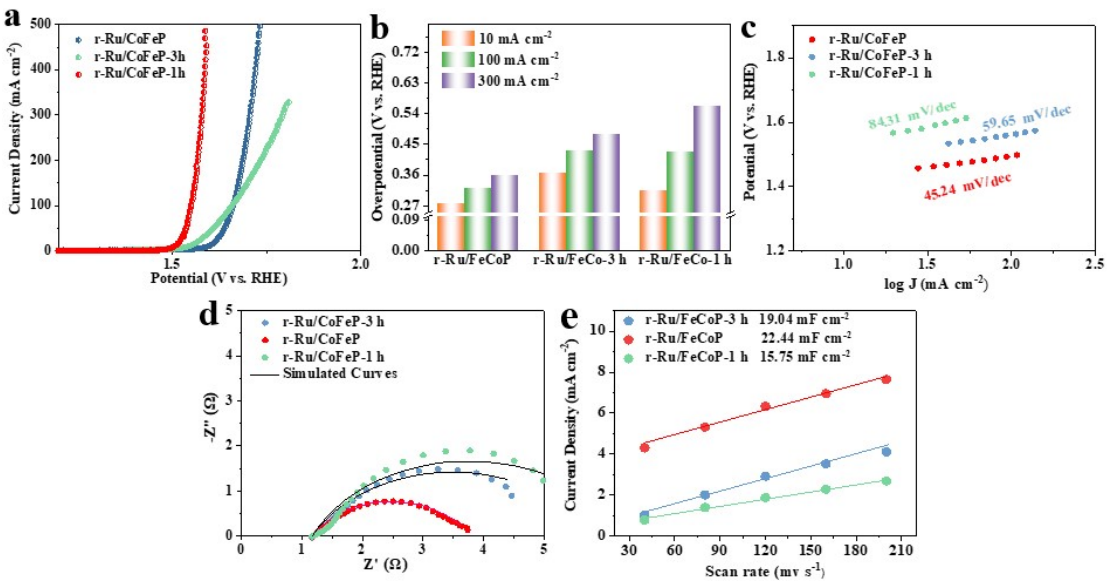

Fig. S17 OER is manifested in 1.0 M KOH. (a) The HER polarization curves of r-Ru/FeCoP, r-Ru/FeCoP-1h, r-Ru/FeCoP-3h in 1.0 M KOH. (b) η_{10}, η_{100}, η_{500} overpotential comparison. (c) Tafel plots of r-Ru/FeCoP, r-Ru/FeCoP-1h, r-Ru/FeCoP-3h. (d) Nyquist plots of r-Ru/FeCoP, r-Ru/FeCoP-1h, r-Ru/FeCoP-3h. (e) The curves of the scanning rate of r-Ru/FeCoP, r-Ru/FeCoP-1h, and r-Ru/FeCoP-3h with capacitance current are shown.

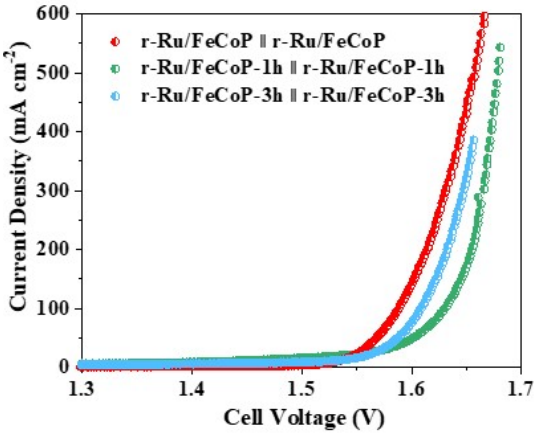

Fig. S18 The total water decomposition diagrams of r-Ru/FeCoP-1h, r-Ru/FeCoP-3h and r-Ru/FeCoP were obtained.

Table S1. The content of Ru element in r-Ru/FeCoP and Ru/FeCoP catalysts obtained by ICP was analyzed.

Electrocatalysts	Ru content (wt %)
Ru/FeCoP	1.202
r-Ru/FeCoP	2.35

Table S2. The fitted R_{ct} value of r-Ru/FeCoP catalyst and other comparative samples for HER and OER.

Electrocatalysts	R_{ct} for HER (Ω)	R_{ct} for OER (Ω)
r-Ru/FeCoP	2.04	2.63
r-Ru/FeCo-LDH	9.82	3.33
Ru/FeCoP	16.82	4.03
FeCoP	38.82	9.83

Table S3. The HER properties of r-Ru/FeCoP at 10 mA cm^{-2} were compared with those of other works of literature.

Electrocatalysts	η_{10} (mv)	Reference
r-Ru/FeCoP	35.6	This work
Ru/HNCS	39	S1
Ru-Co_3O_4	39	S2
Ru-G/CC	40	S3
Ru_2Ni_2 SNs/C	40	S4.
Ru/PNC	40	S5
a-Ru@Co-DHC	40	S6
$Pd_{0.24}Cu_{0.29}Ru_{0.47}$/C	40.7	S7
Ru-CoP/CC	44	S8
Ru-Si	44	S9
Ru-CN-rGO	45	S10
Ru@N/S/TiO2/rGO	50	S11
RuMo/CNT	50	S12
Ru-MoO_2	51	S13
Ru@2H-MoS_2	51	S14
Ru/CoO	55	S15
RuSx/S-GO	58	S16
Ru-HPC	61.6	S17
RuM-C (M= V, Mo, W, Zn, Cu)	65.78	S18
2D-MoO_2/Ru/NC	68	S19
0.5$Ru_{0.1}$Cu-GN1000	68	S20
N-RuS_2/Ru	76	S21
Ru/C_3N_4/C	79	S22
Cu_2xS@RuNPs	82	S23
Ru/$Y(OH)_3$NHs	100	S24

$SrRuO_3$	110	S25
Ru/C	114	S26
Ru@COF-1	200	S27

Table S4. The OER properties of r-Ru/FeCoP at 10 mA cm^{-2} were compared with those of other works of literature.

Electrocatalysts	η_{10} (mv)	Reference
r-Ru/FeCoP	276	This work
Ru-Ni_3S_2	330	S28
Ru@CN	330	S29
Ru/RuO_2-MoO_2-600	333	S30
Ru/N-BP2000	337	S31
Co/RuSAs-N-C	338	S32
$Ni_{1.25}Ru_{0.75}P$	340	S33
Ru-FeRu@C/NC	345	S34
Ru-NiFeLDH	346	S35
1-RuO_2/CeO_2	350	S36
Ru@C_2N	350	S37
Ru_2Ni_2SNs	357	S38
0.4-Ru@NG-750	372	S39
RuPbOx	390	S40
Ru@NG-4	400	S41
$Pt_{53}Ru_{39}Ni_8$	400	S42
NiRuO	410	S43
Ru^0/CeO_2	420	S44
RuSAs-N-C	432	S45
Ru/C-TiO_2	440	S46
Ni/Ru=0.85	457	S47
Ni/Ru=0.36	504	S47
La_2O_3-Gra	570	S48
RuO_2-MoO_2	540	S48
Ru/C	547	S26
Ni/Ru=0.19	570	S47

$Ru–MoO_2$	570	S13
RuCo@NC-600	660	S49

Table S5. The content of Ru element in r-Ru/FeCoP and after HER obtained by ICP was analyzed.

Electrocatalysts	Ru content (wt %)
r-Ru/FeCoP	2.35
r-Ru/FeCoP after HER	2.32

Table S6. Comparison of the potentials of r-Ru/FeCoP‖r-Ru/FeCoP two-electrode and recently reported TMNs two-electrode for overall water splitting at 10 mA cm^{-2} in 1.0 M KOH solution.

Electrocatalysts	η_{10} (V)	References
r-Ru/FeCoP‖r-Ru/FeCoP	1.53	This work
Ru-$NiSe_2$/NF‖Ru-$NiSe_2$/NF	1.537	S50
Ru-RuO_2/Mn‖Ru-RuO_2/Mn	1.54	S51
Co-RuO_2 NWs‖Co-RuO_2 NWs	1.54	S52
Ni_3N/Ru/NCAC‖Ni_3N/Ru/NCAC	1.55	S53
NiO@Ru‖NiO@Ru	1.55	S54
RuP/$CoNiP_4O_{12}$‖RuP/$CoNiP_4O_{12}$	1.56	S55
Ru@BS-5‖Ru@BS-5	1.56	S56
Ru-SA/Ti_3C_2Tx‖Ru-SA/Ti_3C_2Tx	1.56	S57
CoFeRu@C‖CoFeRu@C	1.59	S58
Pt-C/NF//RuO_2/NF‖Pt-C/NF//RuO_2/NF	1.64	S59
RuO_2/Co_3O_4‖RuO_2/Co_3O_4	1.645	S60
Ru-FeCoP‖Ru-FeCoP	1.65	S61

Table S7. The ICP result of Ru element in r-Ru/FeCoP-1h and r-Ru/FeCoP-3h catalysts obtained by ICP was analyzed.

Electrocatalysts	Ru content (wt %)
r-Ru/FeCoP-1h	1.82
r-Ru/FeCoP-3h	2.81

References

S1 H. Du, Z. Du, T. Wang, B. Li, S. He, K. Wang, L. Xie, W. Ai, W. Huang. Unlocking Interfacial Electron Transfer of Ruthenium Phosphides by Homologous Core-Shell Design toward Efficient Hydrogen Evolution and Oxidation. *Adv. Mater* **2022**, *34*, 2204624.

S2 Y. Wang, S. Wang, Z.L. Ma, L.T. Yan, X.B. Zhao, Y.Y. Xue, J.M. Huo, X. Yuan, S.N. Li, Q.G. Zhai. Competitive Coordination-Oriented Monodispersed Ruthenium Sites in Conductive MOF/LDH Hetero-Nanotree Catalysts for Efficient Overall Water Splitting in Alkaline Media. *Adv. Mater,* **2022**, *34*, 2107488.

S3 Y. Jiang, T.W. Huang, H.L. Chou, L. Zhou, S.W. Lee, K.W. Wang, S. Dai. Revealing and magnifying interfacial effects between ruthenium and carbon supports for efficient hydrogen evolution. *J. Mater. Chem. A,* **2022**, *10*, 17730-17739.

S4 Y. Wang, H. Lv, L. Sun, F. Jia, B. Liu. Ordered Mesoporous Intermetallic Trimetals for Efficient and pH-Universal Hydrogen Evolution Electrocatalysis. *Adv. Energy Mater,* **2022**, *12*, 2201478.

S5 J. Cai, J. Yang, X. Xie, J. Ding, L. Liu, W.Y. Liu, Z. Tang, B. Liu, S. Lu. Carbon Doping Triggered Efficient Electrochemical Hydrogen Evolution of Cross-Linked Porous Ru-MoO_2 Via Solid-Phase Reaction Strategy. *Energy Environ. Mater,* **2023**, *6*, e12424.

S6 G.Z. Pu, T. Liu, G. Zhang, Z. Chen, D.S. Li, N. Chen, W. Chen, Z. Chen, S. Sun. General Synthesis of Transition-Metal-Based Carbon-Group Intermetallic Catalysts for Efficient Electrocatalytic Hydrogen Evolution in Wide pH Range. *Adv. Energy Mater,* **2022**, *12*, 2200293.

S7 Q. Liang, Q. Li, L. Xie, H. Zeng, S. Zhou, Y. Huang, M. Yan, X. Zhang, T. Liu, J. Zeng, K. Liang, O. Terasaki, D. Zhao, L. Jiang, B. Kong. Superassembly of Surface-Enriched Ru Nanoclusters from Trapping-Bonding Strategy for Efficient Hydrogen Evolution. *ACS nano,* **2022**, *16*, 7993-8004.

S8 J. Jiao, N.N. Zhang, C. Zhang, N. Sun, Y. Pan, C. Chen, J. Li, M. Tan, R. Cui, Z. Shi, J. Zhang, H. Xiao, T. Lu. Doping Ruthenium into Metal Matrix for Promoted pH-

Universal Hydrogen Evolution. *Adv. Sci*, **2022**, *9*, 2200010.

S9 D. Chen, R. Yu, R. Lu, Z. Pu, P. Wang, J. Zhu, J. Pi, D. Wu, J. Wu, Y. Zhao, Z. Kou, J. Yu, S. Mu. Tunable Ru-Ru_2P heterostructures with charge redistribution for efficient pH-universal hydrogen evolution. *InfoMat,* **2022**, *4*, e12287.

S10 H. Yao, X. Wang, K. Li, C. Li, C. Zhang, J. Zhou, Z. Cao, H. Wang, M. Gu, M. Huang, H. Jiang. Strong electronic coupling between ruthenium single atoms and ultrafine nanoclusters enables economical and effective hydrogen production. *Appl. Catal. B,* **2022**, *312*, 121378.

S11 J. Li, Y. Li, J. Wang, C. Zhang, H. Ma, C. Zhu, D. Fan, Z. Guo, M. Xu, Y. Wang, H. Ma. Elucidating the Critical Role of Ruthenium Single Atom Sites in Water Dissociation and Dehydrogenation Behaviors for Robust Hydrazine Oxidation-Boosted Alkaline Hydrogen Evolution. *Adv. Funct. Mater,* **2022**, *32*, 2109439.

S12 L. Li, L. Bu, B. Huang, P. Wang, C. Shen, S. Bai, T.S. Chan, Q. Shao, Z. Hu, X. Huang. Compensating Electronic Effect Enables Fast Site-to-Site Electron Transfer over Ultrathin RuMn Nanosheet Branches toward Highly Electroactive and Stable Water Splitting. *Adv. Mater,* **2021**, *33*, 2105308.

S13 Y. Wu, W. Wei, R. Yu, L. Xia, X. Hong, J. Zhu, J. Li, L. Lv, W. Chen, Y. Zhao, L. Zhou, L. Mai. Anchoring Sub-Nanometer Pt Clusters on Crumpled Paper-Like MXene Enables High Hydrogen Evolution Mass Activity. *Adv. Funct. Mater,* **2022**, *32*, 2110910.

S14 X. Jin, H. Jang, N. Jarulertwathana, M.G. Kim, S.J. Hwang. Atomically Thin Holey Two-Dimensional Ru_2P Nanosheets for Enhanced Hydrogen Evolution Electrocatalysis. *ACS nano,* **2022**, *16*, 16452-16461.

S15 W. Feng, Y. Feng, J. Chen, H. Wang, Y. Hu, T. Luo, C. Yuan, L. Cao, L. Feng, J. Huang. Interfacial electronic engineering of Ru/FeRu nanoparticles as efficient trifunctional electrocatalyst for overall water splitting and Zn-air battery. *Chem. Eng. J,* **2022,** *437*, 135456.

S16 R. Jiang, Y. Da, J. Zhang, H. Wu, B. Fan, J. Li, J. Wang, Y. Deng, X. Han, W. Hu. Non-equilibrium synthesis of stacking faults-abundant Ru nanoparticles towards electrocatalytic water splitting. *Appl. Catal. B,* **2022**, *316*, 121682.

S17 Z. Pu, J. Zhao, I.S. Amiinu, W. Li, M. Wang, D. He, S. Mu. A universal synthesis strategy for P-rich noble metal diphosphide-based electrocatalysts for the hydrogen evolution reaction. *Energy Environ. Sci,* **2019**, *12*, 952-957.

S18 S. Wang, B. Xu, W. Huo, H. Feng, X. Zhou, F. Fang, Z. Xie, J.K. Shang, J. Jiang. Efficient FeCoNiCuPd thin-film electrocatalyst for alkaline oxygen and hydrogen evolution reactions. *Appl. Catal. B,* **2022**, 313, 121472.

S19 C. Zhou, X. Chen, S. Liu, Y. Han, H. Meng, Q. Jiang, S. Zhao, F. Wei, J. Sun, T. Tan, R. Zhang. Superdurable Bifunctional Oxygen Electrocatalyst for High-Performance Zinc-Air Batteries. *J. Am. Chem. Soc,* **2022**, *144*, 2694-2704.

S20 B. Zhang, J. Shan, X. Wang, Y. Hu, Y. Li. Ru/Rh Cation Doping and Oxygen-Vacancy Engineering of FeOOH Nanoarrays@$Ti_3C_2T_x$ MXene Heterojunction for Highly Efficient and Stable Electrocatalytic Oxygen Evolution. *Small,* **2022**, *18*, 2200173.

S21 H. Song, J. Yu, Z. Tang, B. Yang, S. Lu. Halogen-Doped Carbon Dots on Amorphous Cobalt Phosphide as Robust Electrocatalysts for Overall Water Splitting. *Adv. Energy Mater,* **2022**, *12*, 2102573.

S22 Q. Quan, Y. Zhang, F. Wang, X. Bu, W. Wang, Y. Meng, P. Xie, D. Chen, W. Wang, D. Li, C. Liu, S. Yip, J.C. Ho. Topochemical domain engineering to construct 2D mosaic heterostructure with internal electric field for high-performance overall water splitting. *Nano Energy,* **2022**, *101*, 107566.

S23 X. Zheng, Y. Cao, Z. Wu, W. Ding, T. Xue, J. Wang, Z. Chen, X. Han, Y. Deng, W. Hu. Rational Design and Spontaneous Sulfurization of NiCo-(oxy)Hydroxysulfides Nanosheets with Modulated Local Electronic Configuration for Enhancing Oxygen Electrocatalysis. *Adv. Energy Mater,* **2022**, *12*, 2103275.

S24 H. Su. S. Song, Y. Gao, N. Li, Y. Fu, L. Ge, W. Song, J. Liu, T. Ma. In Situ Electronic Redistribution Tuning of $NiCo_2S_4$ Nanosheets for Enhanced Electrocatalysis. *Adv. Funct. Mater,* **2022**, *32*, 2109731.

S25 M. Gu, X. Deng, M. Lin, H. Wang, A. Gao, X. Huang, X. Zhang. Ultrathin NiCo Bimetallic Molybdate Nanosheets Coated CuO_x Nanotubes: Heterostructure and Bimetallic Synergistic Optimization of the Active Site for Highly Efficient Overall

Water Splitting. *Adv. Energy Mater,* **2021**, *11*, 2102361.

S26 C. Rong, X. Shen, Y. Wang, L. Thomsen, T. Zhao, Y. Li, X. Lu, R. Amal, C. Zhao. Electronic Structure Engineering of Single-Atom Ru Sites via Co-N_4 Sites for Bifunctional pH-Universal Water Splitting. *Adv. Mater,* **2022**, *34*, 2110103.

S27 Y. Song, J. Cheng, J. Liu, Q. Ye, X. Gao, J. Lu, Y. Cheng. Modulating electronic structure of cobalt phosphide porous nanofiber by ruthenium and nickel dual doping for highly-efficiency overall water splitting at high current density. *Appl. Catal. B,* **2021**, *298*, 120488.

S28 V.H. Hoa, D.T. Tran, S. Prabhakaran, D.H. Kim, N. Hameed, H. Wang, N.H. Kim, J.H. Lee. Ruthenium single atoms implanted continuous MoS_2-Mo_2C heterostructure for high-performance and stable water splitting. *Nano Energy,* **2021**, *88*, 106277.

S29 C.B. Hong, X. Li, W.B. Wei, X.T. Wu, Q.L. Zhu. Nano-engineering of Ru-based hierarchical porous nanoreactors for highly efficient pH-universal overall water splitting. *Appl. Catal. B,* **2021**, *294*, 120230.

S30 L. Huang, R. Yao, X. Wang, S. Sun, X. Zhu, X. Liu, M.G. Kim, J. Lian, F. Liu, Y. Li, H. Zong, S. Han, X. Ding. In situ phosphating of Zn-doped bimetallic skeletons as a versatile electrocatalyst for water splitting. *Energy Environ. Sci,* **2022**, *15*, 2425-2434.

S31 Q. Gao, W. Luo, X. Ma, Z. Ma, S. Li, F. Gou, W. Shen, Y. Jiang, R. He, M. Li. Electronic modulation and vacancy engineering of Ni_9S_8 to synergistically boost efficient water splitting: Active vacancy-metal pairs. *Appl. Catal. B,* **2022**, *310*, 121356.

S32 H. Zhang, C. Chen, X. Wu, C. Lv, Y. Lv, J. Guo, D. Jia. Synergistic Incorporating RuO_2 and NiFeOOH Layers onto Ni_3S_2 Nanoflakes with Modulated Electron Structure for Efficient Water Splitting. *Small Methods,* 2022, *6*, 2200483

S33 Zhang H, Aierke A, Zhou Y, Ni Z, Feng L, Chen A, Wågberg T, Hu G. A high-performance transition-metal phosphide electrocatalyst for converting solar energy into hydrogen at 19.6% STH efficiency. *Carbon Energy,* **2022**, *5*, e217.

S34 S. Yan, W. Liao, M. Zhong, W. Li, C. Wang, N. Pinna, W. Chen, X. Lu. Partially oxidized ruthenium aerogel as highly active bifunctional electrocatalyst for overall water splitting in both alkaline and acidic media. *Appl. Catal. B,* **2022**, *307*, 121199.

S35 X. Mu, X. Gu. S. Dai, J. Chen, Y. Cui, Q. Chen, M. Yu, C. Chen, S. Liu, S. Mu.

Breaking the symmetry of single-atom catalysts enables an extremely low energy barrier and high stability for large-current-density water splitting. *Energy Environ. Sci,* **2022**, *15*, 4048-4057.

S36 S.W. Wu, S.Q. Liu, X.H. Tan, W.Y. Zhang, K. Cadien, Z. Li. Ni_3S_2-embedded NiFe LDH porous nanosheets with abundant heterointerfaces for high-current water electrolysis. *Chem. Eng. J,* **2022**, *442*, 136105.

S37 P. Zhai, M. Xia, Y. Wu, G. Zhang, J. Gao, B. Zhang, S. Cao, Y. Zhang. Z. Li, Z. Fan, C. Wang, X. Zhang, J.T. Miller, L. Sun, J. Hou. Engineering single-atomic ruthenium catalytic sites on defective nickel-iron layered double hydroxide for overall water splitting. *Nat. Commun,* **2021**, *12*, 4587.

S38 S. Yang, J.Y. Zhu, X.N. Chen, M.J. Huang, S.H. Cai, J.Y. Han, J.S. Li. Self-supported bimetallic phosphides with artificial heterointerfaces for enhanced electrochemical water splitting. *Appl. Catal. B,* **2022**, *304*, 120914.

S39 L. Bai, Z. Duan, X. Wen, R. Si, Q. Zhang, J. Guan. Highly dispersed ruthenium-based multifunctional electrocatalyst. *ACS Catalysis*, 2019, 9, 9897-9904

S40 Huang R, Wen Y, Peng H, Zhang B. Improved kinetics of OER on Ru-Pb binary electrocatalyst by decoupling proton-electron transfer. *Chinese Journal of Catalysis*, **2022**, 43, 130-138.

S41 B.K. Barman, D, Das, K.K. Nanda. Facile synthesis of ultrafine Ru nanocrystal supported N-doped graphene as an exceptional hydrogen evolution electrocatalyst in both alkaline and acidic media. *Sustainable Energy & Fuels*, **2017**, 1, 1028-1033.

S42 Y.C. Shi, T. Yuan, J.J. Feng, J. Yuan, A.J. Wang. Rapid fabrication of support-free trimetallic $Pt_{53}Ru_{39}Ni_8$ nanosponges with enhanced electrocatalytic activity for hydrogen evolution and hydrazine oxidation reactions. *Journal of colloid and interface science*, **2017**, 505, 14-22.

S43 S. Datta, F. Pettersson, S. Ganguly, H. Saxén, N. Chakraborti. Designing high strength multi-phase steel for improved strength–ductility balance using neural networks and multi-objective genetic algorithms. *ISIJ international*, **2007**, 47, 1195-1203.

S44 S. Akbayrak, Y. Tonbul, S. Özkar. Ceria-supported ruthenium nanoparticles as

highly active and long-lived catalysts in hydrogen generation from the hydrolysis of ammonia borane. *Dalton Transactions*, **2016**, 45, 10969-10978.

S45 Z. Han, P. Wu, M. He, X. Zhuang, H. Lin, S. Han. Ammonia synthesis by electrochemical nitrogen reduction reaction-A novel energy storage way. *Journal of Energy Storage*, **2022**, 55, 105684.

S46 H. Zhang, G. Li, R. Nie, X. Lu, Q. Xia. One-pot synthesized mesoporous C-TiO_2 hybrid for Ru-catalyzed low-temperature hydrogenation of benzoic acid. *Journal of Materials Science*, **2019**, 54, 7529-7540.

S47 S. Zhou, L. Jin, P. Gu, L. Tian, N. Li, D. Chen, A. Marcomini, Q. Xu, J. Lu. Novel calixarene-based porous organic polymers with superfast removal rate and ultrahigh adsorption capacity for selective separation of cationic dyes. *Chemical Engineering Journal*, **2022**, 433, 134442.

S48 D. Wang, L. Jin, M. Liu, T.G. Lee, S.G. Peera, C. Liu. The graphene-supported Lanthanum oxide cluster as efficient bifunctional electrocatalyst for oxygen reaction. *Molecular Catalysis*, **2023,** 535, 112879.

S49 F. Zhang, Y. Zhu, Y. Chen, Y. Lu, Q. Lin, L. Zhang, S. Tao, X. Zhang, H. Wang. RuCo alloy bimodal nanoparticles embedded in N-doped carbon: a superior pH-universal electrocatalyst outperforms benchmark Pt for the hydrogen evolution reaction. *Journal of Materials Chemistry A*, **2020**, 8, 12810-12820.

S50 R. Qin, P. Wang, Z.L. Li, J.X. Zhu, F Cao, H W Xu, Q.L. Ma, J.Y. Zhang, J. Yu. MuRu-Incorporated Nickel Diselenide Nanosheet Arrays with Accelerated Adsorption Kinetics toward Overall Water Splitting. *Small*, **2021**.

S51 X. Xie, X. Zhang, W. Tian, X. Zhang, J. Ding, Y. Liu, S. Lu. Tri-functional Ru-RuO2/Mn-MoO2 composite: A high efficient electrocatalyst for overall water splitting and rechargeable Zn–air batteries. *Chemical Engineering Journal*, **2023**,468,143-760.

S52 J. Wang, Y. Ji, R. Yin, Y. Li, Q. Shao, X. Huang. Transition metal-doped ultrathin RuO2 networked nanowires for efficient overall water splitting across a broad pH range. *Journal of Materials Chemistry A*, 2019, 7, 6411-6416.

S53 X. Zhao, X. Yong, Q. Ji, Z. Yang, Y. Song, Y. Sun, Z. Cai, J. Xu, L. Li, S. Shi, F. Chen, C. Li, P. Wang, J.-B. Baek. Controlled synthesis of highly active bifunctional

electrocatalysts for overall water splitting using coal-based activated carbons. *Journal of Materials Chemistry A*, 2023, 11, 12726-12734.

S54 L. Zhang, Z. Hu, H. Li, Q. Ren, S. Hu. Nickel Foam Supported NiO@Ru Heterostructure towards High-fficiency Overall Water Splitting. *Chem Phys Chem*, **2021**.

S55 J. Zhao, Y. Zhang, Y. Xia, B. Zhang, Y. Du, B. Song, H.-L. Wang, S. Li, P. Xu, Strong phosphide-metaphosphate interaction in $RuP/CoNiP_4O_{12}$ for enhanced electrocatalytic water splitting. *Applied Catalysis B*, **2023**, 328 122-447.

S56 S. Tang, Z. Liu, F. Qiu, Q. Liu, Y. Mao, L. Zhang. The active ruthenium (101) crystal plane selectively exposed by in situ metal hyperaccumulation on a living plant for overall water splitting. *Green Chemistry*, **2022**, 24 9668-9676.

S57 S. Yang, J.-Y. Zhu, X.-N. Chen, M.-J. Huang, S.-H. Cai, J.-Y. Han, J.-S. Li. Self-supported bimetallic phosphides with artificial heterointerfaces for enhanced electrochemical water splitting. *Applied Catalysis B*, **2022**, 304, 120914.

S58 M. Yang, T. Feng, Y. Chen, J. Liu, X. Zhao, B. Yang. Synchronously integration of Co, Fe dual-metal doping in Ru@C and CDs for boosted water splitting performances in alkaline media. *Applied Catalysis B*, **2020**, 267, 118657.

S59 H. Liu, X. Ma, H. Hu, Y. Pan, M. Wu. Robust NiCoP/CoP Heterostructures for Highly Efficient Hydrogen Evolution Electrocatalysis in Alkaline Solution. *ACS Applied Materials & Interfaces*, **2019**, 11.

S60 Q. Su, R. Sheng, Q. Liu, J. Ding, P. Wang, X. Wang, J. Wang, Y. Wang, B. Wang, Y. Huang. Surface reconstruction of RuO_2/Co_3O_4 amorphous-crystalline heterointerface for efficient overall water splitting. *Journal of Colloid and Interface Science*, **2023**.

S61 L. Zhang, X. Cao, C. Guo, A. Hassan, Y. Zhang, J. Wang. Interface and morphology engineering of Ru-FeCoP hollow nanocages as alkaline electrocatalyst for overall water splitting. *Journal of Environmental Chemical Engineering*, **2023**, 11, 111373.